Microspectroscopy and imaging using a delay line detector in time-of-flight photoemission microscopy

A. Oelsner,[a] O. Schmidt, M. Schicketanz, M. Klais, and G. Schönhense
Institut für Physik, Johannes Gutenberg Universität Mainz, 55099 Mainz, Germany

V. Mergel, O. Jagutzki, and H. Schmidt-Böcking
Institut für Kernphysik, Johann Wolfgang von Goethe Universität, 60486 Frankfurt, Germany

(Received 13 November 2000; accepted for publication 29 July 2001)

A method for microspectroscopy and energy-selective imaging using a special photoemission electron microscope (PEEM) is presented. A modified commercial PEEM was combined with a delay line device as *x, y, t* detector serving as the basic arrangement for spectromicroscopy. One can measure the time of flight of the electrons passing a drift section in order to analyze the energy distribution of photoelectrons in PEEM. The time of flight is referenced to the time structure of the synchrotron radiation from an electron storage ring. At electron kinetic energies of less than 20 eV within the drift region a spatial resolution of about 100 nm has been obtained. Fast counting electronics (instead of a camera) delivers an image for real-time monitoring on an oscilloscope screen or for image acquisition by a computer. A time resolution of about 500 ps has been obtained with the potential of further improvement. The spatial resolution of the delay line detector is about 50 μm in the image plane corresponding to 1000 pixels in the image diagonal. Direct photoemission from the W-4*f* core level of a W(110) single-crystal sample was observed at several photon energies. The W-4*f* fine-structure splitting of 2.3 eV could be well resolved at a pass energy around 40 eV through the drift region. © *2001 American Institute of Physics.* [DOI: 10.1063/1.1405781]

I. INTRODUCTION

The ability of structural and chemical object differentiation with high lateral resolution has proven microscopy with photoelectrons to be a very powerful tool. Since the first photoemission electron microscope (PEEM) experiments of Brüche *et al.*[1–4] the method has established for different applications, particularly in surface physics, chemistry, and the material sciences. In the parallel imaging approach, the lateral photoelectron intensity distribution is viewed by an electron-optical lens system analogously to an optical microscope.

In the conventional operation modes of the PEEM low energy photons are used for the excitation (that are UV gas discharge or Hg high-pressure lamps). The image contrast results from a lateral variation of the electron yield mainly as a consequence of local differences of the work function, variation of the crystalline structure as well as the surface topography. This mode of UV-PEEM is characterized by the excitation of electrons from the valence band in the vicinity of the Fermi level. Hence, only very limited information on the chemical composition of the imaged sample is obtained, because the chemical information cannot be extracted unambiguously from the value of the work function or the magnitude of the electron yield. Nevertheless, the work function contrast has been exploited with great success in the study of the spatiotemporal evolution of catalytic reactions at surfaces.[5]

A chemically more sensitive technique is the combination of PEEM with x-ray absorption spectroscopy (XAS), pioneered by Tonner and Harp.[6] The excitation with synchrotron radiation of variable energy obtains element specific information by choosing a suitable photoabsorption edge of the selected element. In the imaging process, the secondary electron yield is exploited which is a measure of the photoabsorption signal. The creation of a hole in an inner shell by photoexcitation of an electron to an unoccupied state is followed by an Auger deexcitation. These Auger electrons cause a secondary electron cascade due to inelastic processes. Finally, the signal of the true secondary electrons is observed. It increases if the photon energy reaches an absorption edge. Thus, the range of applications of a PEEM.[6–11] can be extended considerably using tunable synchrotron radiation as an illuminating source. The photon energy can be scanned across the regions of the absorption edges of the elements constituting a sample while detecting the electron yield. This mode of XAS microspectroscopy directly reveals the chemical distribution. In certain cases the XANES features (x-ray absorption near edge structure) allow even a selective imaging of the same element in different chemical states as was recently demonstrated for graphitic and diamond-like carbon films.[12,13]

This undoubtedly very powerful method has shortcomings in those cases where there is no access to a strong absorption edge. For instance the energy region of typical grazing-incidence monochromators covers about $h\nu = 100-1500$ eV. These energies are not sufficient to image transition metals like Pt and Au, whose $M_{4,5}$ edges are well beyond 2000 eV. Consequently, it is almost impossible to detect as much as a few monolayers of Pt on top of a mag-

[a]Electronic mail: oelsner@mail.uni-mainz.de

netic sandwich structure[14,15] (by using the very weak N_3 edge). On the contrary, it is no problem to detect 0.1 monolayers of Cr with good chemical contrast utilizing the strong $L_{2,3}$ white lines.[14,16] Thus, if we are restricted to the soft x-ray range, the use of XAS is not as general as the use of x-ray photoelectron spectroscopy (XPS), also termed electron spectroscopy for chemical analysis (ESCA).

In view of these shortcomings of XAS, there are several approaches to combine lateral imaging with XPS.[17] The ESCASCOPE[18] basically combines an electron energy analyzer with an imaging lens system and is characterized by an ultimate resolution of a few microns, i.e., not sufficient for nanoanalytical purposes. Higher resolution is obtained by small-spot ESCA,[19,20] where the lateral resolution is obtained by focusing the x-ray beam onto the sample or by selecting a small area via the electron optics.[21,22] Due to the scanning mode of operation the image acquisition is relatively slow. In the third approach, an imaging energy filter is implemented into an electron microscope column. Two such systems have been in operation,[23–25] another two are under development.[26–28] These X-PEEM instruments can reach very high resolution in the 30 nm range.[23] They pose, however, a considerable challenge to the experimentalists due to a complicated, nonlinear electron optical system.

A much simpler way to add the capability for ESCA has been introduced by Spiecker *et al.*[29] Here the time-of-flight (TOF) technique, well known in spectroscopy,[30,31] was implemented into a PEEM. The necessary time resolution was obtained by using a camera with an ultrafast gated optical intensifier. The technique was limited by the low efficiency and the decay time of the scintillator material used for the imaging screen. It reached an overall time resolution of about 1.4 ns thus impairing high resolution spectroscopy.

In this article we present a new and highly effective approach to TOF-PEEM by using a space- and time-resolving delay line detector.[32–34] A lateral resolution of 100 nm has been obtained which is not limited by the detector. In the first experiments the time resolution was about 500 ps with the potential of further improvement. In contrast to the experiment using the gated camera (setting a time-of-flight, i.e., energy interval) the delay line detector collects all electrons arriving at different times. Since it is based on single-electron counting it is characterized by an ultimate detection sensitivity. Like in conventional X-PEEM, it makes use of the well-known techniques of UPS and XPS combined with PEEM in order to investigate images with element specific information at a fixed photon energy. In addition, a future challenge is to increase the spatial resolution of the electron microscope by reducing the chromatic aberration.

II. EXPERIMENTAL SETUP

The new method for energy-selective imaging is based on a modified PEEM system in combination with a time- and space-resolving detector thus establishing a TOF-PEEM. Some details of the design are similar to the instrument described in Ref. 29. Here, we combined the FOCUS IS-PEEM[8] with a ROENTDEK delay line detector.[32–34] This technique allows a very fast two-dimensional position

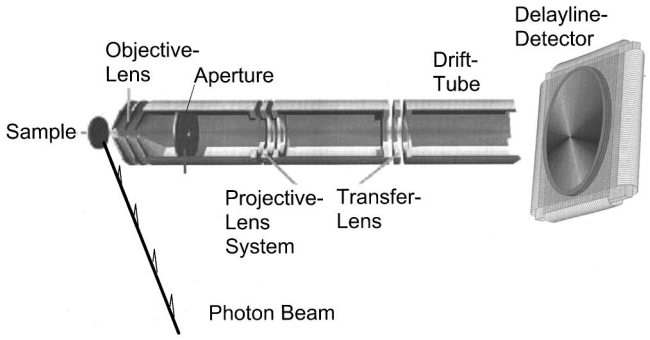

FIG. 1. Schematic view of the PEEM equipped with transfer lens, drift tube, and delay line detector for time- and space resolved detection.

imaging with computer-supported signal processing. The delay line detector can be used instead of a CCD camera and has a superior time resolution in the sub-nanosecond range. In addition, its working principle is based upon single-electron counting thus yielding maximum detection efficiency.

The PEEM is a three-lens electrostatic photoemission microscope comprising a tetrode objective lens, an adjustable contrast aperture (variable size from 500 to 30 μm), and two projective lenses. As schematically shown in Fig. 1, the rear part of the PEEM column was used as a drift tube at reduced potential, where electrons are retarded to the drift energy of about 20–80 eV, required for a detectable time/energy dispersion. To analyze the energy distribution of photoelectrons in PEEM, the time of flight for electrons passing this section is measured, referenced to the time structure of a pulsed photon source, in our case the synchrotron radiation. This mode is similar to spectroscopic TOF experiments.[30,31] The investigations were carried out at the monochromator PM-III of the Berlin storage ring BESSY-I in the photon energy range from $h\nu = 100$ to 1000 eV. The photon incidence angle was 65° with respect to the surface normal. The time structure of the synchrotron radiation provides short light pulses with an effective duration time below 600 ps (Ref. 35) and a period of repetition of about 208 ns in the single-bunch mode. The maximum detection time of 208 ns between two bunches sets a limit to the detection of electrons with low kinetic energies within the drift region. The time of flight for electrons of a certain start energy can be varied by using a sample bias or a variable voltage at the drift tube. This is advantageous in order to select the desired energy resolution and to optimize the setting for different regions of the energy distribution of photoelectrons.

The principle of the image detection is schematically illustrated in Fig. 2. Each electron, after passing the drift region with a certain energy impinges on the multichannel-plate (chevron arrangement of two plates) inducing locally a secondary electron avalanche. The charge cloud from the MCP stack crosses the meander-like delay line wound around a base plate (for one dimension schematically shown in Fig. 2). The charge pulse induces an electric pulse on the wires which propagates to the ends x_1 and x_2 of the wires with speed of light. An electronic clock measures the signal arrival time at each end. The time interval $\Delta\tau_x$ is proportional to the respective position of the charge cloud in the x

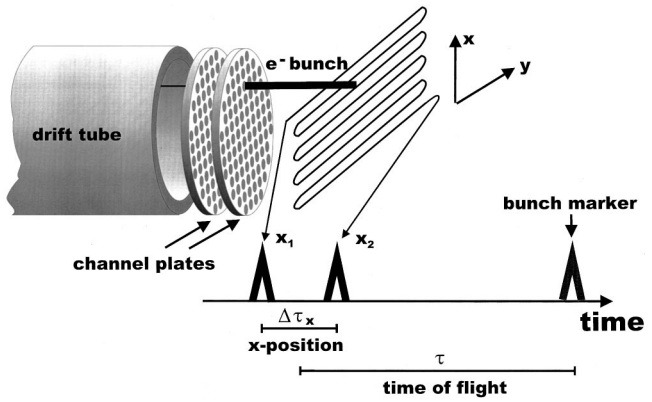

FIG. 2. Detection principle of the delay line detector. The x position is derived from the time delay $\Delta\tau_x$ of the arrival time at the two ends x_1 and x_2 of the delay line. The TOF is derived from the arrival time of the center of the two signals at x_1 and x_2 with respect to the bunch marker. A second delay line behind the first one being azimuthally rotated by 90° yields the same information for y.

direction. For the y direction the same arrangement is used but rotated azimuthally by 90°. This position encoding using the delay line method has many advantages as compared to charge dividing methods. The electronic readout is considerably simpler and allows a higher spatial resolution. Maximum acquisition rates in the MHz regime and even multihit events can be processed with commercially available electronics. The arrangement of two crossed delay lines yields, together with a pulse amplification electronics as well as a time to digital conversion unit (TDC), time resolved two-dimensional images. For each event, this is attained by determination of the center of the two signals x_1 and x_2 with respect to the time reference of the exciting photon source (bunch marker, see Fig. 2). A fast histogram storage device enables a high data transfer rate after the detection and an image monitoring in real time with an integrated two channel digital to analog conversion (DAC) for the use of a conventional oscilloscope.

The main advantage of this approach in contrast to our earlier experiment[29] (defining a certain time interval for detection) is that it provides a simultaneous acquisition of all electrons passing the microscope. This is achieved by direct detection and storage of the x, y, t ''coordinates'' of all electrons arriving at the delay line detector. The time resolution depends only on the specifications of the detector itself, in contrast to the method reported in Ref. 29, where the decay time of the PMMA-scintillator screen turned out to be the major limiting contribution.

III. TIME AND SPATIAL RESOLUTION

Using the equations given by Spiecker *et al.*[29] we have calculated the theoretical energy versus time resolution of the present device. The achievable energy resolution of the described TOF-spectro-microscope depends mainly on the length of the drift tube used and the drift energy defined by the retardation potential at its entrance. For the transit time in the PEEM-lens regions the situation is more complicated. The minimum energy of all electrons in the other sections of the device is about 800 eV, so for electrons with drift energies below 100 eV we have neglected all contributions of the high-energy part of the lens system. In this experiment, we used a drift tube with a length $L_d = 400$ mm.

The electron time of flight (TOF) depends on the drift energy E_d as shown in the double logarithmic plot of Fig. 3. We find a TOF below 200 ns for drift energies above 10 eV. This TOF is close to the upper limit in our experiments which is given by the single bunch period of 208 ns at the used synchrotron radiation source BESSY-I. The second line in Fig. 3 shows the dispersion $dE/d\tau$ for a certain drift energy. One can estimate an energy resolution of 10 meV for the drift energy of 10 eV by use of a detection system with a time resolution of 100 ps. In this article we will show measurements which were taken at a time resolution of 500 ps using drift energies of about 40 eV. In this case, we reached a resolution limit of about 450 meV. Nevertheless, we have successfully performed the imaging at drift energies down to $E_d = 5$ eV using device parameters like in the conventional PEEM mode. This mode was not applied in our TOF experiments, because its maximum TOF exceeds the detection window of 208 ns (BESSY-I single bunch period). In the future this mode will be available using the time structured modes

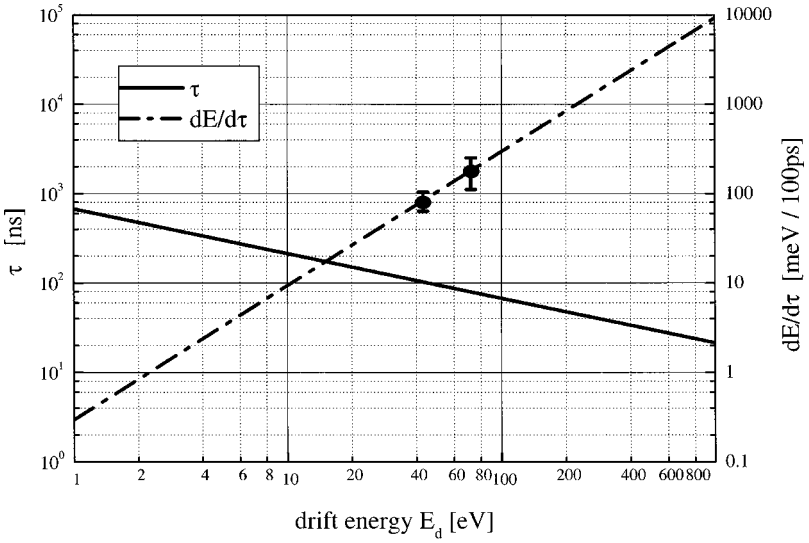

FIG. 3. Calculation of TOF τ as well as dispersion dE/dt vs drift energy E_d for the conditions used in the experiments. The error bars are corresponding to two prominent measurements, done in x-ray photoemission from W(110) (see Fig. 7).

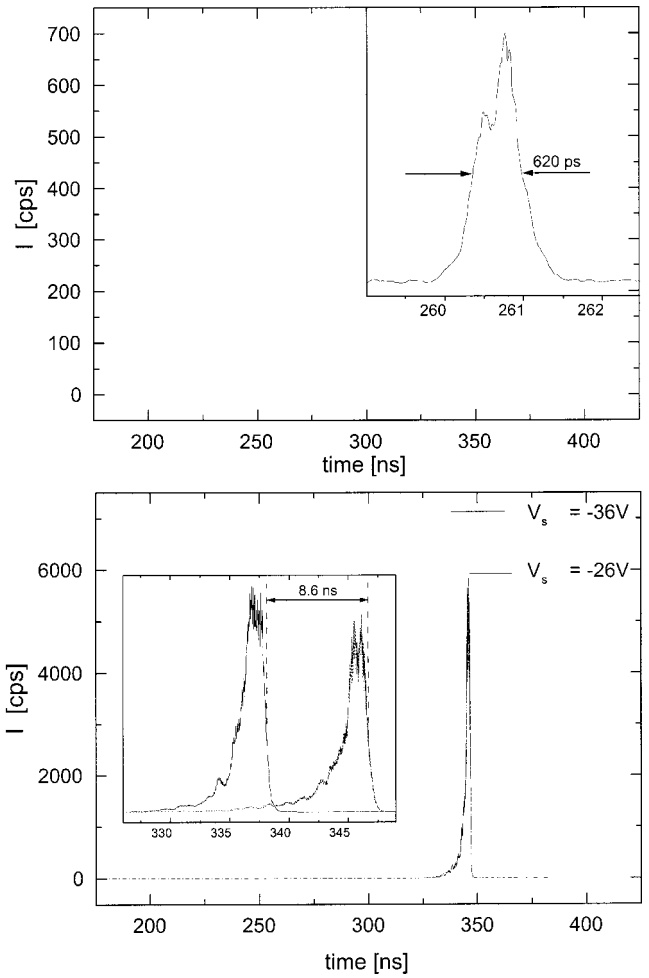

FIG. 4. Time resolution measurements: direct detection of photons (top) and electron signals (bottom) using different sample bias.

at the new Berlin synchrotron source BESSY-II. Here, we expect a period of about 400 or 800 ns in a double bunch mode or in a single bunch mode, respectively. The minimum drift energy can be chosen down to 5 eV or below using these modes. Therefore, we expect much progress in the enhancement of the energy resolution limit of TOF-PEEM using high performance readout electronics.

The best calibration in TOF measurements can be achieved by detection of scattered photons from synchrotron radiation in zero-order mode of the monochromator. Suppressing the photoelectrons completely by a suitable voltage, a weak photon structure becomes visible in the time spectra. It marks a good reference point for measurements of the energy distribution of the photoelectrons. The upper inset of Fig. 4 shows the photon peak in detail revealing a FWHM of 620 ps. This is a typical timing resolution for the detector, however, a new prototype delay line detector already yielded 200 ps.[36] The detection principle of the delay line detector determines both the hitting position of the electron at the detector and the TOF through the microscope from the same signal time measurement. Therefore, the temporal resolution for the TOF determination can approximately reach the device limit, measuring the event position at the detector simultaneously. The TDC used provides a best timing resolution of

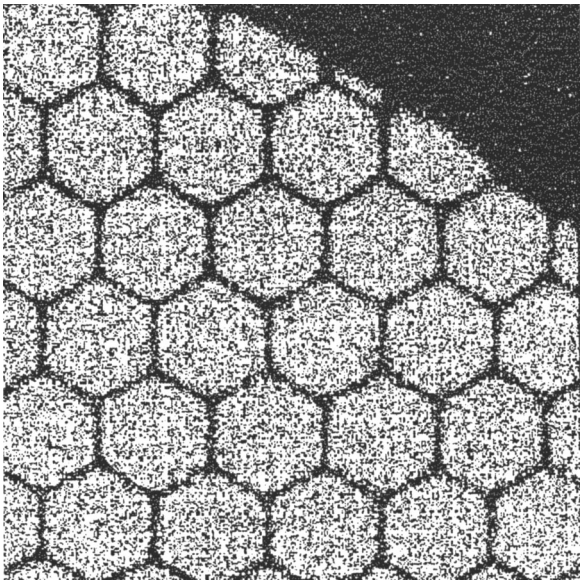

FIG. 5. Spatial resolution test using a shadow mesh in front of the detector (linewidth: 0.2 mm, period: 3 mm).

120 ps. The resolution of the delay line is negligibly small in comparison.

Typical TOF electron spectra for soft x-ray excitation are shown in the lower inset of Fig. 4. It is possible to shift the spectra by varying the sample bias voltage in order to optimize the time resolution in the region of interest. We were able to get a high spatial resolution in the operation modes with kinetic energies of less then 20 eV within the drift region. With respect to the nonretarding mode no changes in resolution have been observed in appropriate tests with a conventional image unit.

The delay line detector provides its spatial resolution independently of a time structure of the incoming electrons. Therefore, the device may be used also for PEEM investigations by means of a continuous-wave irradiation as shown in the following examples. An example image for a measurement of the spatial resolution of the delay line detector used is shown in Fig. 5. Note that this is not an image of a sample, it was measured with a homogeneous irradiation using a shadow mesh (line width 200 μm, period 3 mm) in front of the detector. In this way, a resolution of 47 μm has been obtained. Given the active detector diameter of 47 mm, this corresponds to 1000 pixels per image diameter and is thus directly comparable to the common technique using a typical CCD camera. An image taken by the TOF-PEEM with a delay line detector using a Hg-discharge lamp is shown in the left inset of Fig. 6. The sample surface consists of stripes of Pd on Si with a period of 3.7 μm. A line scan was made perpendicular to the stripe orientation as indicated by the straight line. The result is shown in the right inset of Fig. 6. The line scan reveals a spatial resolution of less than 100 nm in the PEEM mode using the delay line detector.

IV. APPLICATION IN MICROSPECTROSCOPY AND ENERGY-SELECTIVE IMAGING

The time of flight τ is directly related to the transit energy E_d of the electrons in the drift tube of length L_d by

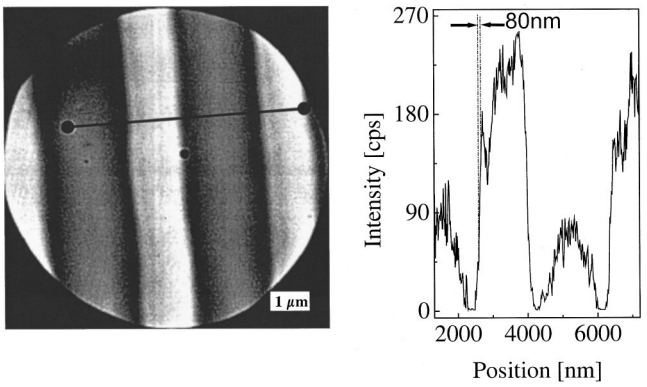

FIG. 6. PEEM image of a Si sample with a regular stripe structure from Pd (periodicity 3.7 μm), taken with the delay line detector, using a Hg-discharge lamp in threshold photoemission. The line scan at the right-hand side is taken perpendicular to the stripes in the marked region.

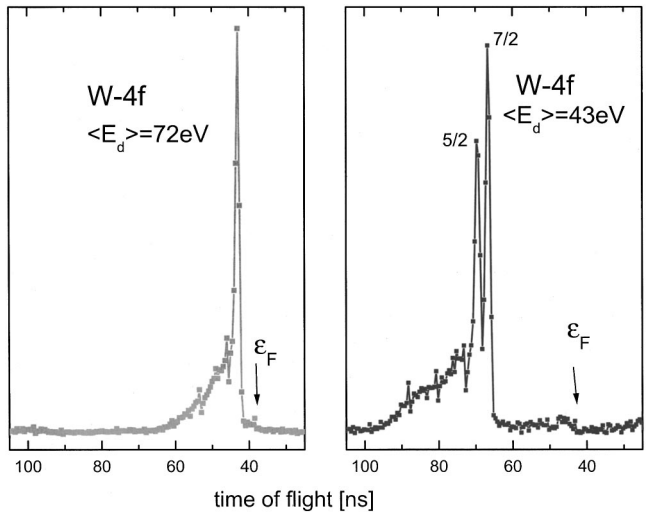

FIG. 7. Photoelectron spectra of W-4f emission from a W(110) single crystal. Note that the energy resolution increases for the lower center kinetic energy of W-4f electrons.

$\tau = L_d(2E_d/m_e)^{-1/2}$ with m_e being the electron mass. Thus, the TOF method facilitates an energy analysis of the photoelectrons from microselected areas at any sample investigated by means of the PEEM. Consequently, the TOF-PEEM may be used for XPS investigations with high lateral resolution. It has to be mentioned that the energy resolution can only be constant for such XPS measurements when a ''constant bandpass'' mode is used. In this case, the time interval between the detection time window and the light pulse has to be constant. In this mode either the sample potential or the drift-tube potential must be swept in order to measure the energy distribution. In contrast, an advantage of our approach (TOF-PEEM by means of the delay line detector) is given by the use of the fast histogram storage device. The system may register every photoelectron within a large time window and count it into the corresponding memory channel. This takes place independently on the electron's drift time but is limited by the period length of the photon source ($T = 208$ ns). The use of this option enables the highest data acquisition rate, which is essentially restricted by the transfer speed between TDC and histogram storage device ($\sim$1 MHz for the present setup). In this operation mode, photoelectron spectra must not be taken step by step sweeping a retarding voltage but may be extracted from the histogram dataset after a suitable analysis. This detection mode has no real analog in comparison with a common dispersive analyzer. However, it does not provide a constant energy resolution across the spectrum (see also Fig. 3 and discussion).

In order to demonstrate the varying energy resolution, the direct photoemission from the W-4f core level of a W(110) single crystal sample was observed at two different photon energies (see Fig. 7). The kinetic energy of photoelectrons within the drift tube depends not only on the photon energy and the binding energy, but also on the potential difference between sample and drift tube, thus allowing to select the energy resolution in the regions of interest. It can clearly be seen from Fig. 7 that the lower drift energy results in much better energy resolution of the W-4f doublet. From the right spectrum one can reproduce the binding energy of the W-4f electrons of 31.4 and 33.6 eV and the spin-orbit splitting well, whereas at 72 eV average drift energy the resolution is not sufficient to resolve the fine structure splitting. The experimentally determined energy resolutions are plotted as error bars in Fig. 3.

In addition, in these spectra one can observe a further advantage of the delay line detector, that is the superior signal-to-background ratio in comparison with a conventional image intensifier that consists of multichannel-plate (MCP), phosphor screen and CCD camera. The latter contains two sources of dark counts, that is the MCP and the CCD camera. In addition, the pulse-height distribution of the MCP is converted at the phosphor into an intensity distribution. In our approach, the dark counts contribute only the MCP. The system counts all events above a selected threshold independently on the pulse height distribution. Every dark-count event contributes to the background being uncorrelated in time and therefore appears smeared out over the hole duty cycle of 208 ns, while the time interval of the spectrum might be only 10 ns. The same occurs with respect to the scattered electrons in the electrostatic device. Thus, it is possible to achieve a better signal-to-background ratio in comparison to experiments, where no temporal correlation is made.

Although the energy resolution decreases rapidly for high drift energies E_d of the electrons (Fig. 3), one can obtain enough information for chemical analysis from XPS with TOF-PEEM. One example is shown in Fig. 8, measured at a photon energy of $h\nu = 780$ eV. The sample was a meteorite fragment prepared using a flash heating procedure in UHV only. As expected, one observes photoemission from iron (Fe $2p$), oxygen (O $1s$), and carbon (C $1s$). These features can clearly be assigned although the resolution is low at high kinetic energies. According to Fig. 3 the carbon $1s$ line at a kinetic energy of 530 eV has an expected width of 7.2 eV.

One of the challenges for TOF-PEEM measurements is to exploit the method as a powerful tool for energy-selective imaging. Like imaging in ESCA, element specific information can be extracted from this application. In addition, the chromatic aberrations of the microscope may be reduced by

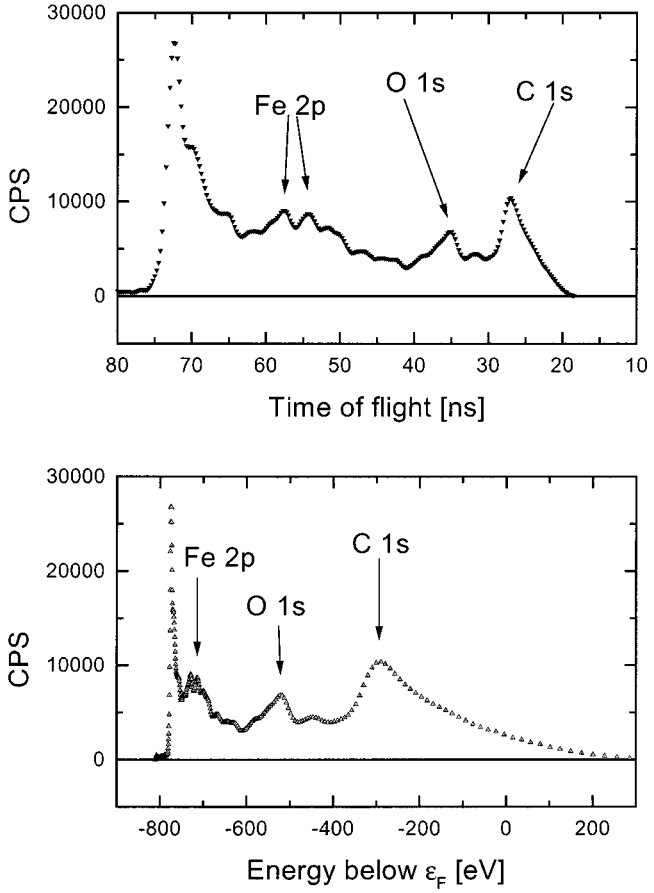

FIG. 8. Wide-range XPS spectrum from a meteorite fragment sample at $h\nu = 780$ eV.

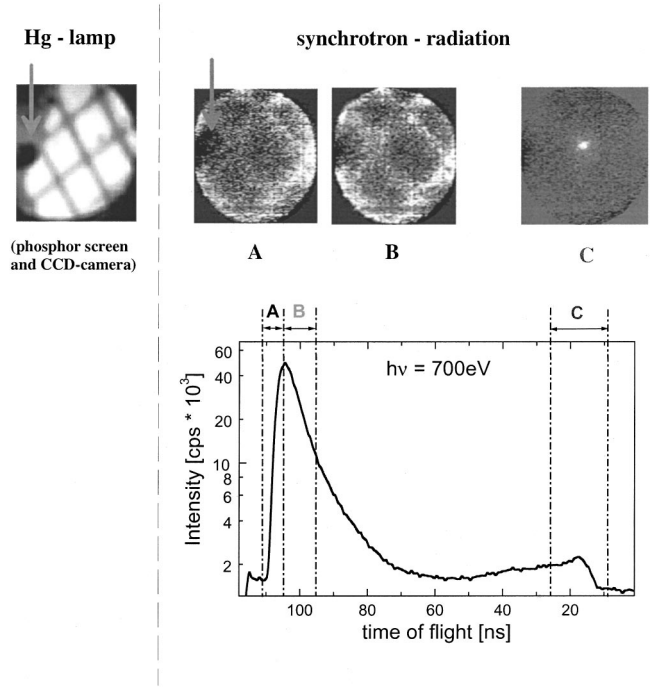

FIG. 9. Energy-selective imaging of a structured Fe layer on Si. The images were taken at the low energy cutoff (A), the secondary electrons (B), and at the Fermi edge (C) of the photoelectron spectrum.

selecting a narrow energy interval for imaging. Here, we demonstrate the energy selective imaging by measurements at a structured Fe/Si sample. The results are shown in Fig. 9. At a photon energy of $h\nu = 700$ eV the energy distribution is 695 eV wide like shown in the spectrum in Fig. 9. We could not find any structure in the image integrated over the complete spectrum in contrast to the reference measurement with a Hg-discharge lamp (left-hand side image). The energy selection allows to observe the expected structure from the electrons at low kinetic energies (images A and B). Only the image A shows the marked feature, which is apparently given by a work function contrast.

From electrons close to the Fermi edge (image C) only a bright spot is observed. It points out the fact that electrons with high kinetic energies are totally out of the instrument's focus. With other words, an imaging with high lateral resolution is only possible for a narrow energy band applying the above discussed mode. Nevertheless, the size of the field of view may be chosen approximately constant (in the few μm range) for a wide-range spectrum of kinetic energies. That enables to measure a wide-range XPS spectrum in defined microselected areas. On the one hand, the focusing condition can be chosen free for one certain energy of interest within such spectra leading to a high resolution image (<100 nm) at the chosen energy. On the other hand, the defocusing effects can be largely neglected for the above-discussed "microspectroscopy" mode with μm resolution.

V. CONCLUSIONS AND OUTLOOK

The TOF-PEEM method using a delay line detector is dedicated to measure electron dispersion in photoelectron microscopy in an elegant way. We have shown, that spectromicroscopy can be done using time of flight analysis. A time resolution of some 100 ps is currently accessible. Without changing the microscope size, and retaining a linear electron-optical axis, it is possible to obtain energy resolutions of about 100 meV, using drift energies of 50 eV or less. The method needs to reference the electron signal to the time structure of the excitation source but opens at the same time an additional application field for PEEM investigations. Without using additional equipment, the described device can be used for stroboscopic experiments like known from the pump probe technique.[37] The use of the delay line detector replaces the CCD camera and therefore two conversions of the signal (at the fluorescent screen and in the CCD) are not needed anymore. Thereby, the spatial resolution of the delay line detector is about 50 μm in the image plane being equivalent to 1000 pixels in the image diagonal in the case of the current design. The energy selective imaging provides element specific information by using a single excitation energy. In the future, the chromatic aberrations of the microscope may be reduced. To reach this aim, a possible solution is given by an adjustment of the electrical field in the electron-optical elements dynamically.

The energy-selective imaging can be improved even by optimizing the used electron optics. Only the low energy fraction of all emitted electrons is used in conventional operation modes of PEEM. The requirements to the electron optics are different for the imaging of electrons with high kinetic energies. Thus, there is a large potential for enhance-

ment of spectral analysis in using this type of electron optics.

We are confident, that this technique will lead to a new quality of X-PEEM measurements using synchrotron radiation. In particular, the discrimination of several kinds of contrast will improve the interpretation of the results maintained in PEEM experiments in the x-ray range. Also, the instrument gives access to the sub-ns time scale, which is in general of interest for the observation of dynamic processes obtained on solid surfaces.

ACKNOWLEDGMENTS

The authors thank all members of the BESSY crew for good collaboration during the beamtimes. Financial support by the BMBF (05 SC8UMA 0) is gratefully acknowledged.

[1] E. Brüche and H. Johannson, Z. Phys. **33**, 898 (1932).
[2] E. Brüche, Z. Phys. **86**, 448 (1933).
[3] J. Pohl, Z. Techn. Phys. **15**, 579 (1934).
[4] H. Mahl and J. Pohl, Z. Techn. Phys. **16**, 219 (1935).
[5] For a review, see, R. Imbihl and G. Ertl, Chem. Rev. **95**, 697 (1995).
[6] B. P. Tonner and G. R. Harp, Rev. Sci. Instrum. **59**, 853 (1988).
[7] J. Stöhr, Y. Wu, B. D. Hermsmeier, M. G. Samant, G. R. Harp, S. Koranda, D. Dunham, and B. P. Tonner, Science **259**, 658 (1993).
[8] W. Swiech, G. H. Fecher, Ch. Ziethen, O. Schmidt, G. Schönhense, K. Grzelakowski, C. M. Schneider, R. Frömter, H. P. Oepen, and J. Kirschner, J. Electron Spectrosc. Relat. Phenom. **84**, 171 (1997).
[9] F. U. Hillebrecht, D. Spanke, J. Dresselhaus, and J. Solinus, J. Electron Spectrosc. Relat. Phenom. **84**, 189 (1997).
[10] G. Margaritondo, Scanning Spectromicrosc. **9**, 949 (1995).
[11] G. H. Fecher, Y. Hwu, and W. Swiech, Surf. Sci. **377–379**, 1106 (1997).
[12] Ch. Ziethen, O. Schmidt, G. K. L. Marx, G. Schönhense, R. Frömter, J. Gilles, J. Kirschner, C. M. Schneider, and O. Gröning, J. Electron Spectrosc. Relat. Phenom. **107**, 261 (2000).
[13] Ch. Ziethen, O. Schmidt, G. H. Fecher, C. M. Schneider, G. Schönhense, R. Frömter, M. Seider, K. Grzelakowski, M. Merkel, D. Funnemann, W. Swiech, H. Gundlach, and J. Kirschner, J. Electron Spectrosc. Relat. Phenom. **88–91**, 983 (1998).
[14] C. M. Schneider, R. Frömter, Ch. Ziethen, W. Swiech, N. B. Brookes, G. Schönhense, and J. Kirschner, Mater. Res. Soc. Symp. Proc. **475**, 381 (1997).
[15] C. M. Schneider, J. Magn. Magn. Mater. **175**, 160 (1997).
[16] C. M. Schneider, R. Frömter, Ch. Ziethen, W. Swiech, N. B. Brookes, G. Schönhense, and J. Kirschner, International Colloquium on Magnetic Films and Surfaces (ICMFS), Brisbane, Australian, Conference Digest, 132, 1977.
[17] H. Ade, J. Electron Spectrosc. Relat. Phenom. **84**, 1 (1997).
[18] E. Adem, R. Champaneria, and P. Coxon, Vacuum **41**, 7 (1990).
[19] Brochure Quantum 2000, Physical Electronics (PHI), Elen Prairie, MN, Brochure ESCALAB 2201-XL, Vacuum Generators (VG), East Grinstead, Sussex, GB; Brochure Axis Ultra, Kratos Analytical (Shimadzu).
[20] Voss *et al.*, in Ref. 17.
[21] O. Schmidt, Ch. Ziethen, G. H. Fecher, M. Merkel, M. Escher, D. Menke, U. Kleineberg, U. Heinzmann, and G. Schönhense, J. Electron Spectrosc. Relat. Phenom. **88–91**, 1009 (1998).
[22] U. Kleineberg, D. Menke, F. Hamelmann, U. Heinzmann, O. Schmidt, G. H. Fecher, and G. Schönhense, J. Electron Spectrosc. Relat. Phenom. **101–103**, 931 (1999).
[23] E. Bauer, C. Koziol, G. Lilienkamp, and T. Schmidt, in Ref. 17 p. 201.
[24] T. Schmidt *et al.*, Surf. Rev. Lett. **5**, 1287 (1988).
[25] B. P. Tonner, D. Dunham, T. Droubay, and M. Pauli, in Ref. 17, p. 211.
[26] G. K. L. Marx, V. Gerheim, and G. Schönhense, in Ref. 17, p. 251.
[27] R. Fink, M. R. Weiss, E. Umbach, D. Preikszas, H. Rose, R. Spehr, P. Hartel, W. Engel, R. Degenhardt, R. Wichtendahl, H. Kuhlenbeck, W. Erlebach, K. Ihmann, R. Schlögl, H.-J. Freund, A. M. Bradshaw, G. Lilienkamp, Th. Schmidt, E. Bauer, and G. Benner, J. Electron Spectrosc. Relat. Phenom. **84**, 231 (1997).
[28] R. Wichtendahl *et al.*, Surf. Rev. Lett. **5**, 1249 (1998).
[29] H. Spiecker, O. Schmidt, Ch. Ziethen, D. Menke, U. Kleineberg, R. G. Ahuja, M. Merkel, U. Heinzmann, and G. Schönhense, Nucl. Instrum. Methods Phys. Res. A **406**, 499 (1998).
[30] N. Saito, F. Heiser, O. Hemmers, K. Wieliczek, J. Viefhaus, and U. Becker, Phys. Rev. A **54**, 2004 (1996).
[31] G. Snell, M. Drescher, N. Müller, U. Heinzmann, U. Hergenhahn, and U. Becker, J. Phys. B **32**, 2361 (1999).
[32] I. Ali, R. Dorner, O. Jagutzki, S. Nuttgens, V. Mergel, L. Spielberger, Kh. Khayyat, T. Vogt, H. Brauning, K. Ullmann, R. Moshammer, J. Ullrich, S. Hagmann, K.-O. Groeneveld, C. L. Cocke, and H. Schmidt-Bocking, Nucl. Instrum. Methods Phys. Res. B **149**, 490 (1999).
[33] R. Mooshammer, M. Unverzagt, W. Schmitt, J. Ullrich, and H. Schmidt-Böcking, Nucl. Instrum. Methods Phys. Res. B **108**, 425 (1996).
[34] J. Ullrich, R. Dörner, V. Mergel, O. Jagutzki, L. Spielberger, and H. Schmidt-Böcking, Comments At. Mol. Phys. **30**, 285 (1994).
[35] B. Winter *et al.*, BESSY Annual Report (1998), p. 492.
[36] V. Mergel (private communication).
[37] O. Bostanjoglo and M. Weingärtner, Rev. Sci. Instrum. **68**, 2456 (1997).